Polymer Testing 120 (2023) 107961

Contents lists available at ScienceDirect

Polymer Testing

journal homepage: www.elsevier.com/locate/polytest

AFM monitoring of the cut surface of a segmented polyurethane unveils a microtome-engraving induced growth process of oriented hard domains

Hubert Gojzewski [a,*], Martin van Drongelen [b], Balazs Imre [c], Mark A. Hempenius [a], Casey Check [d], Richard Chartoff [e], Frederik R. Wurm [a], G. Julius Vancso [a,f,**]

[a] Sustainable Polymer Chemistry, Department of Molecules & Materials, Faculty of Science and Technology, University of Twente, 7522 NB, Enschede, the Netherlands
[b] Production Technology, Faculty of Engineering Technology, University of Twente, 7522 NB, Enschede, the Netherlands
[c] Department of Physical Chemistry and Materials Science, Budapest University of Technology and Economics, 1111, Budapest, Hungary
[d] Center for Advanced Materials Characterization in Oregon (CAMCOR), University of Oregon, Eugene, OR, 97405, USA
[e] School of Chemical Biological and Environmental Engineering, Oregon State University, Corvallis, OR, 97331, USA
[f] Materials Science and Technology of Polymers, Faculty of Science and Technology, University of Twente, 7522 NB, Enschede, the Netherlands

ARTICLE INFO

Keywords:
Polyurethane
PeakForce AFM
Microtoming
Oriented hard domains
Temperature

ABSTRACT

We report on nanoscale order-disorder transitions of hard segments and their domains composed of 4,4′-methylenebis(phenyl isocyanate) - 1,4-butanediol (MDI-BD), in polycaprolactone-based (M_n = 2000 g/mol) polyurethanes (PCL-PUs), when the free surface is pre-oriented by cryo-microtoming of the material. Morphological variations of the hard domains as a function of temperature and the anisotropy of surface morphology features are captured by employing Atomic Force Microscopy (AFM) stiffness imaging by PeakForce Quantitative Nanomechanical Mapping (PF-QNM). The AFM imaging is supported by WAXS, SAXS, FTIR, and DSC measurements. The experimental results show that hard domains initially grown at the surface break apart at elevated temperatures (65 °C) and cannot be re-grown upon cooling. They require new microtoming to repeat the growth scenario. The detailed step-by-step submicron scale observations of the surfaces serve to show importance of the influence that microtoming and the time after its completion have on surface morphology, and that these shall be considered when studying polymer materials microscopically.

1. Introduction

Segmented polyurethanes (PU) are fascinating multiblock copolymer materials displaying a plethora of interesting morphologies and useful properties. This richness is due to the broad range of possible chemical structures of the repeat units connected by urethane groups in the macromolecules [1]. Soft and hard segments, and their diverse polarity and stiffness, contribute to a multitude of different thermoplastic elastomers due to their aggregating in phases of varied separation domains [1–6]. The elastomeric character is due to the soft phase being in a rubbery elastic state (with glass transition temperature, T_g, below ambient), while the hard phase being glassy (with T_g above ambient) or crystalline serves as reversible crosslinking points. Above a certain temperature, the hard phase melts/becomes rubbery, enabling the polymer to flow [7]. Soft segments are often composed of oligomeric or polymeric diols that feature flexible chains, i.e., polyethers, polyesters, or polycarbonates, and exhibit sub-ambient glass transition temperatures. The hard segments can be derived from aromatic or aliphatic diisocyanates and low molar mass diols. Regarding the microphase morphologies, the size and shape of the phase-separated domains depend on the interplay between chain conformation, cohesive energy density, entropy of formation, and interfacial energy of the microstructures. Thus the mechanical behavior of PUs is difficult to predict *'ab initio'* [1,3,8]. PUs may also be interesting candidates as engineering materials for the future, conforming to recent trends to enhance the share of biobased and biodegradable polymers for the circular economy [9–11]. For instance, polycaprolactone (PCL), often employed as a soft segment in PUs is a biodegradable elastic polyester, which is also of high interest for medical applications [10,12].

Atomic Force Microscopy (AFM) is one of the platform techniques

* Corresponding author.
** Corresponding author. Sustainable Polymer Chemistry, Department of Molecules & Materials, Faculty of Science and Technology, University of Twente, 7522 NB, Enschede, the Netherlands.
E-mail addresses: h.gojzewski@utwente.nl (H. Gojzewski), g.j.vancso@utwente.nl (G.J. Vancso).

https://doi.org/10.1016/j.polymertesting.2023.107961
Received 28 December 2022; Received in revised form 28 January 2023; Accepted 5 February 2023
Available online 9 February 2023

that is widely used to study the surface structure and properties of polymers across the length scales from nanometres to hundreds of micrometers [13,14]. It has been used with great success to determine polyurethane microphase separation, domain morphology, and nanomechanical properties [15,16]. A significant improvement in the visualization of polyurethane surface morphologies has been achieved by the use of the Tapping Mode [17–20], and more recently, by PeakForce Quantitative Nanomechanical Mapping (PF-QNM) [5,21,22]. PF-QNM is a high-resolution technique not only capable of visualizing morphology, but also provides quantitative information on the mechanical characteristics (stiffness, adherence) of the respective micro- and nanophases at the specimen's surface and sub-surface regions.

AFM has also been used with success to monitor morphology variations that accompany temperature-dependent phase transitions [23–26]. However, phase transitions and ordering at surfaces can be significantly different due to relaxation effects at free surfaces, or contact with liquids [27]. Little is known about the nature of morphology transitions at the PUs surface as distinct from the bulk behavior. The question thus arises: to what extent do the surface and surface morphology transitions differ from the bulk? To determine this, it is of particular interest to employ temperature-dependent PF-QNM to investigate surface rearrangements in PUs.

Temperature-dependent physical behavior forms the basis for advanced PU applications. For example, Kim et al. prepared PCL-based PUs with shape memory capabilities [28]. They showed that the variation of the soft and hard phases, and the molecular interactions present at different temperatures, drive the shape memory effect. A recent study demonstrated that the relative amount of the PCL phase in PCL-based PUs affect the material's ability to self-heal [29]. These studies show that PCL-based PUs can be functional biomaterials responding to temperature and time.

In this work, we use PUs obtained from 4,4′-methylenebis(phenyl isocyanate) (MDI), 1,4-butanediol (BD) and ε-polycaprolactone diol (PCL) with a constant stoichiometric ratio of the isocyanate and hydroxyl groups and a constant stoichiometric ratio of polymer diol to total diol component. We aim at investigating surface mechanical behavior, morphology changes, and detecting structural variations during phase transitions, as a function of temperature. The material of choice for these AFM investigations contained 20 mol% of the polyester diol with respect to total diol content. We observe the formation and destruction of hard, ordered domains at varying temperatures using AFM employed in the PF-QNM mode. We discuss the formation of such oriented domains when the free surface is pre-oriented by microtoming of the material. We complement the experiments by X-ray diffraction (WAXD, SAXS; main text), and spectroscopy (FTIR; Supporting Information) as well as thermal analysis (DSC; Supporting Information) to contrast bulk and surface property variations.

2. Experimental

2.1. Polyurethane synthesis and sample preparation

Phase-separated polyurethane samples, PU_{PCL}, were synthesized according to a procedure detailed elsewhere [21] with 0.20 M ratio of PCL (M_n = 2000 g/mol, Sigma-Aldrich) with respect to total diols and BD (Alfa Aesar) at the stoichiometric ratio (1.01) of the isocyanate and hydroxyl groups, respectively, with the content of the hard segments of 32.2 wt%. The chemical structure of the PU_{PCL} is shown in Scheme 1.

Two other samples as references for differential scanning calorimetry (DSC), namely, PU_{100} with 100% soft segments (without BD), and PU_0 with 100% hard segments (without PCL), were also investigated (Supporting Information). PCL was dried under vacuum at 100 °C for 3 h before use. BD was distilled under vacuum and stored over activated 0.4 nm molecular sieves. MDI (Sigma-Aldrich) flake was used without further purification. N,N-dimethylformamide (DMF, Sigma-Aldrich) was dried over activated silica gel pellets, distilled over freshly powdered, activated silica gel at reduced pressure, and stored over activated 0.4 nm molecular sieves until use.

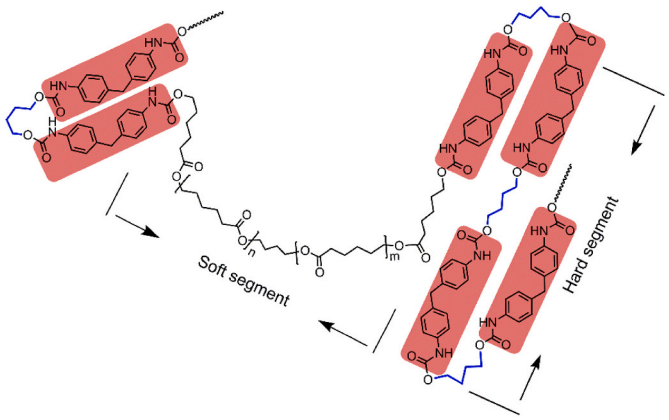

Scheme 1. Chemical structure of the PU_{PCL} studied in this work. The PU_{PCL} was synthesized from 4,4′-methylenebis(phenyl isocyanate) (MDI), 1,4-butanediol (BD) and poly(ε-caprolactone diol) (PCL).

2.2. Wide- and small-angle X-ray scattering

Wide Angle X-ray Diffraction (WAXD) and Small Angle X-ray Scattering (SAXS) experiments were performed on a Bruker D8 Discover System. A Cu-source was used with X-ray wavelength of 0.154 nm and a 2D Eiger R500K detector was employed at either ~40 mm (WAXD) or ~400 mm (SAXS) from the sample. Montel optics provided a highly parallel beam which was collimated at 0.2 mm in diameter. In the case of SAXS experiments, the beam path was partially evacuated to remove air scattering.

WAXD patterns of the sample were obtained in the transmission mode by clamping the sample onto the centre stage of the X-Ray Diffraction (XRD) system. A measurement time of 3 min was used per WAXD scan. A background scan measurement was subtracted to compensate for environmental scattering. The pattern was radially integrated to obtain intensity, I, versus the scattering angle, 2θ.

SAXS patterns were acquired in transmission mode also during stepwise heating of the sample. For this purpose, a Linkam THMS600 temperature stage was installed in the beam path. The temperatures of investigation were in the range between 30 and 95 °C, with higher data point density (smaller temperature increase increment) between 55 and 65 °C. The sample was wrapped in polyimide foil and pressed against the heating element within the stage to ensure proper thermal contact. The temperature was maintained at a set temperature for 20 min for conditioning, prior to a 12.5-min acquisition of SAXS patterns. The sample was heated to the subsequent set temperature at a rate of 50 °C/min. A background measurement was subtracted from all SAXS patterns to compensate for the remaining environmental scattering and the PI foil used. All patterns were radially integrated to obtain intensity, I, versus scattering vector, q. An average spacing was determined from the integrated data using $L = 2\pi/q_{max}$, where q_{max} is the scattering vector with maximum scattering intensity.

2.3. AFM sample preparation

First, the samples were compression molded at 215 °C and allowed to solidify from the melt in between press platens that were cooled by circulating cooling water (15–20 °C) over 10 min, thus forming solid surfaces with no previous shear history [30]. Second, microtoming was used, which inevitably provides mechanical shear and thus knife mark anisotropy at the sample surface. To expose PU_{PCL} bulk surfaces for quantitative AFM imaging, cryo-microtoming (Ultracut EM-FCS, Leica) was performed. Samples were cut in small pieces (approx. 0.5 × 1.0 × 2

mm^3), mounted on a sample holder, and cooled with liquid N_2 to −140 °C. A glass knife at 45° cutting angle was used for a final sample cutting at 70 nm increments, with a sliding speed of 0.1 mm/s. The sample procedure was applied for the re-microtomed samples. This procedure produced a sample surface with low roughness and stress within the sample so that a detailed multiphase morphology could be observed under AFM. As-prepared samples were adhesion fastened to an aluminum sample-holder using a silver conductive paint (SCP03G, Electrolube). The silver conductive paint covered all sides of the samples along with the disc surface to obtain the best possible thermal conductance between the samples and heater.

2.4. AFM sample sets

To study the temperature- and surface-initiated dispersion and growth of the hard domains, five sample sets were considered for the AFM imaging, i.e.: **(set 1)** prior to microtoming, scanned at RT; **(set 2)** microtomed, scanned at temperatures within the range of 21–65 °C; **(set 3)** microtomed, scanned at temperatures within the range of 65–160 °C; **(set 4)** microtomed, heated up to 65 °C, cooled down to RT and scanned at RT; **(set 5)** sample set (4) that was then re-microtomed, and scanned again at RT. Sample sets (1), (2) and (5) are of primary interest in the main article text. Sample sets (3) and (4) are briefly discussed in the Supporting Information. Note, whenever mentioned in the text, a sample was (re)microtomed, it was microtomed at cryo-temperatures (−140 °C).

2.5. PF-QNM imaging as a function of temperature

Commercial Multimode 8 AFM with NanoScope V controller was used in the PeakForce Quantitative Nanomechanical Mapping (QNM) mode (Bruker) to obtain a series of images representing the topography and contact elastic modulus values (hereinafter called Young's modulus) of the PU_{PCL} samples. In the QNM mode, images are collected monitoring force-distance curves while tapping; thus, shear forces during imaging are essentially eliminated. The surface is raster-scanned, and at every image pixel the tip-sample distance and penetration upon contact is driven by a sine-wave piezo signal at a given frequency up to the peak-force amplitude value [31,32]. Due to the viscoelastic behavior of the PU_{PCL} samples at high temperatures, we chose to image at 1 kHz piezo frequency rate and within the range of 150–250 nm of the peak-force amplitude. To detect the cantilever deflection, particularly when deforming mechanically compliant polyurethane surfaces, an appropriate choice of cantilever stiffness must be made. We used uncoated soft cantilevers with a nominal spring constant of 0.5 N/m terminated by a pyramidal silicon uncoated tip of ~8 nm in radius (HQ: NSC19/No Al, MicroMasch). The values of the individual cantilever spring constants were determined by the thermal tune method [33,34]. Values ranging from 0.21 to 0.26 N/m were obtained.

The temperature of the specimens was regulated by a Thermal Applications Controller (TAC 1, Bruker) connected to a high-temperature heater (High-T, Bruker) that was placed on top of a vertical engagement scanner (JV-HC, Bruker). To ensure thermal stability of the scanner during heating and scanning, a water-cooling system with a control unit (Masterflex L/S 77,200–12, Cole-Parmer Instrument Co.) and a peristaltic pump (Masterflex 7016–20, Cole-Parmer Instrument Co.) were employed. As a result, the temperature of the scanner was kept at room temperature, while samples were heated up. The samples' heating rate was set at 5 °C/min. The temperature of the samples was additionally checked and confirmed by an infrared thermometer (62 MAX, Fluke) after a 10 min thermal stabilization period at each temperature step. The accuracy of the AFM imaging at elevated temperatures is discussed in the Supporting Information.

To evaluate the AFM mechanical responses of PU_{PCL} samples in the QNM mode, two approaches were employed. These were the Derjaguin, Muller, and Toporov (DMT) model of contact mechanics and the "relative modulus determination method" [21,35,36]. To quantify the surface stiffness by the second approach, an AFM calibration with an elasticity reference sample is required. For this purpose, a commercial polydimethylsiloxane (PDMS) film reference material (Bruker) was used: an average Young's modulus value was set at 3.5 MPa [37]. The calibrated AFM was then used for the determination of the surface effective Young's moduli values of the PU_{PCL} samples. Modulus determination was obtained by adjusting the applied peak-force values, also for samples studied at elevated temperatures, to obtain similar average indentation depths as were performed for the PDMS reference (the ScanAsyst functionality in the NanoScope software was set to be "individual"). Image processing and data analysis were conducted with the NanoScope (ver. 8.15) and the NanoScope Analysis software (version 1.9), respectively.

3. Characterization results

3.1. WAXD and SAXS

WAXD and SAXS experiments were performed in the bulk to complement surface-related AFM structural information. WAXD data for the PU_{PCL} sample reveal a broad scattering peak, like those found in the case of fully amorphous polymers (Fig. 1a). An average repeat distance or d-spacing value, of 0.42 nm ± 0.08 nm was obtained. The average correlated spacing values, determined from the SAXS peak position, q_{max}, are shown in Fig. 1b. With temperature, q_{max} averages around a value of 0.5 nm^{-1}, which correlates to structural features with a spacing of ca. 12 nm. A slight growth of feature size values was observed with increasing temperature.

3.2. AFM

Set 1: Morphology at room temperature (non-microtomed). We first describe and discuss results obtained at RT (21 °C) on compression molded surfaces that have not been microtomed. The surface of these materials did not experience a shear prior to solidification. Representative scans are captured in Fig. 2. As the hard domains are poorly visible in the height image, a peak force error (PF-QNM feedback signal) image is presented as well that better emphasizes the surface texture (note that the *z*-scale in this image has no physical meaning).

A simple model of the PU_{PCL} can be used to describe the surface observed structures. Hard domains (indicated by white circles in Fig. 2) are composed of aligned and ordered "whiskers" [21]. "Whiskers" are mainly composed of ordered MDI-BD hard segments, which stack as shown in Scheme 2 (stacking is within the red rods). The order is orientational, no three-dimensional symmetry is present. The size of the hard domains (Fig. 2) is limited (smaller than 100 nm). Single "whiskers" are 10–15 nm in width, but of different lengths. The observation of the width of the "whiskers" corroborates previous calculations of hard segment length [21,30]. The long axis of the "whiskers" corresponds to the orientation of the segments in the hard domains (Scheme 2). This implies the anisotropic character of the hard domains, in general.

Set 2: Morphology at room temperature (microtomed). Subsequently, we turned our attention to imaging surfaces investigated at RT (21 °C) following microtoming. The free surface of these samples has been exposed to shear forces during microtoming (Fig. 3). Fig. 3a shows a surface spot from which an area of 2 μm × 2 μm was selected that contained large hard domains (Fig. 3b and c). The surface structure unveils a distinct phase-separated morphology, both seen in the height image (Fig. 3b) and in the Young's modulus maps (Fig. 3c). The Young's modulus mean value varies, from 25 MPa for the soft phase and increases up to around 120 MPa for the largest visible hard domain (Fig. 3c). This fits to the range of the Young's modulus values reported earlier for similar systems [5]. Stiffness in these domains is mainly provided by the MDI units connected by the short aliphatic chains of BD. Also, the fairly polar urethane groups are present in a much higher

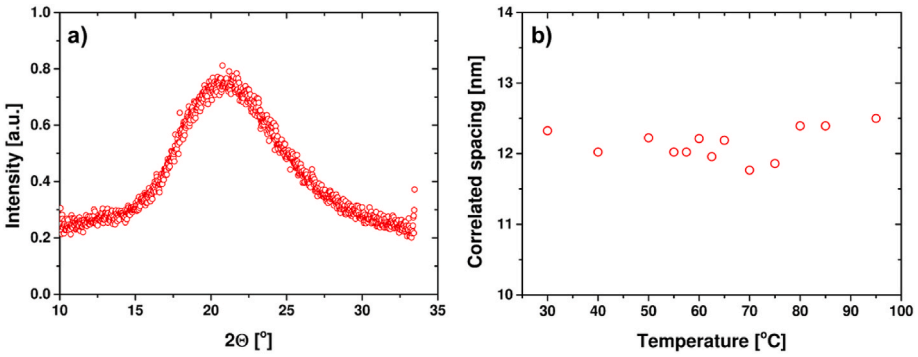

Fig. 1. (a) Radially integrated WAXD pattern intensity at room temperature; (b) SAXS average correlated spacing values determined from the peak position, q_{max}, at elevated temperatures.

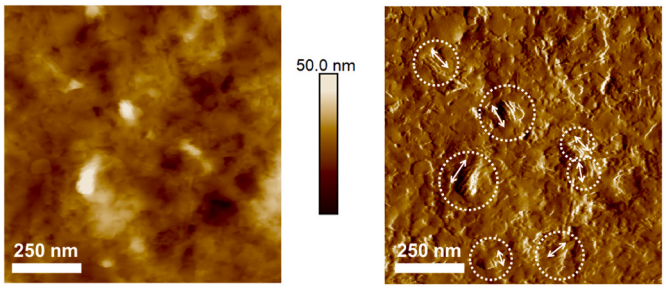

Fig. 2. AFM height (left) and peak force error (right) images captured for the free surface (non-microtomed) of the PU_{PCL} sample at RT temperature. Scan size is 1 μm × 1 μm. The dashed circles indicate the hard domains composed of "whiskers"; white arrows indicate the orientation of the "whiskers".

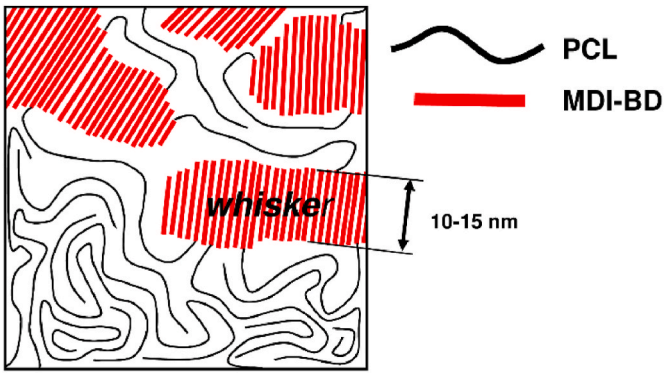

Scheme 2. Schematic of the PU_{PCL} bulk surface structure: MDI-BD hard segments stack (red rods) to form "whiskers". Note, the scheme is simplified to two-dimensional packing.

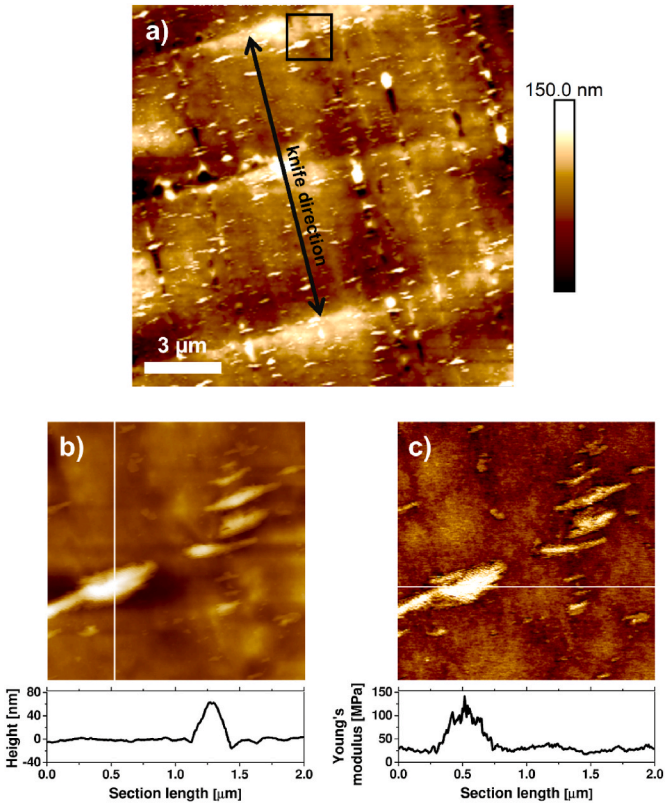

Fig. 3. AFM (a, b), height image, and (c) Young's modulus map captured at room temperature (21 °C) for the PU_{PCL} sample following microtoming. Areas (b) and (c) (2 μm × 2 μm) were selected from image (a) (15 μm × 15 μm) (indicated by a square). The cross-sections were taken along the white lines.

density, leading to more intra- and intermolecular interactions in the hard domains. We note that similar results were shown previously [21].

The arrow in Fig. 3a indicates the direction of knife movement during microtoming. As can be observed, the hard domains have grown perpendicular to the knife movement direction. Another example of the AFM height image is presented in the Supporting Information (Fig. S1).

Set 2: Morphology at 25 – 62.5 °C (sample microtomed). Fig. 4 shows Young's modulus maps obtained at the same spot as captured in Fig. 3c, while the temperature was increased from 25 to 62.5 °C. The surface morphology starts to change above 25 °C. Data captured shows that small hard domains decrease in size in response to increasing temperature. Young's modulus values clearly decrease at 35 °C for both the soft and the hard phase (see the cross-section analysis in Fig. 5). A representative example for this change is indicated by grey arrows in Fig. 4.

Above 40 °C all medium-sized and large hard domains visibly start to reduce in size, from their circumference inwards, as well. An example is shown in Fig. 4 by black arrows (see also Figs. S2 and S3 in the Supporting Information). The disintegration of the hard domains is anisotropic: slow along the microtome cutting direction, but fast perpendicular to this direction. A noticeable drop of Young's modulus is observed above 40 °C (Fig. 5), from 22.3 ± 9.9 MPa, through 13.7 ± 3.9, to 8.7 ± 3.2 MPa at 40, 45, and 50 °C, respectively. From 50 °C on the Young's modulus value decreases slightly (Fig. S7 in the Supporting Information).

Around 60 °C, the remaining hard domains begin to break down. At 65 °C (and above, as shown in Fig. S5 in the Supporting Information), hard domains are not seen by the AFM anymore. At this temperature, the

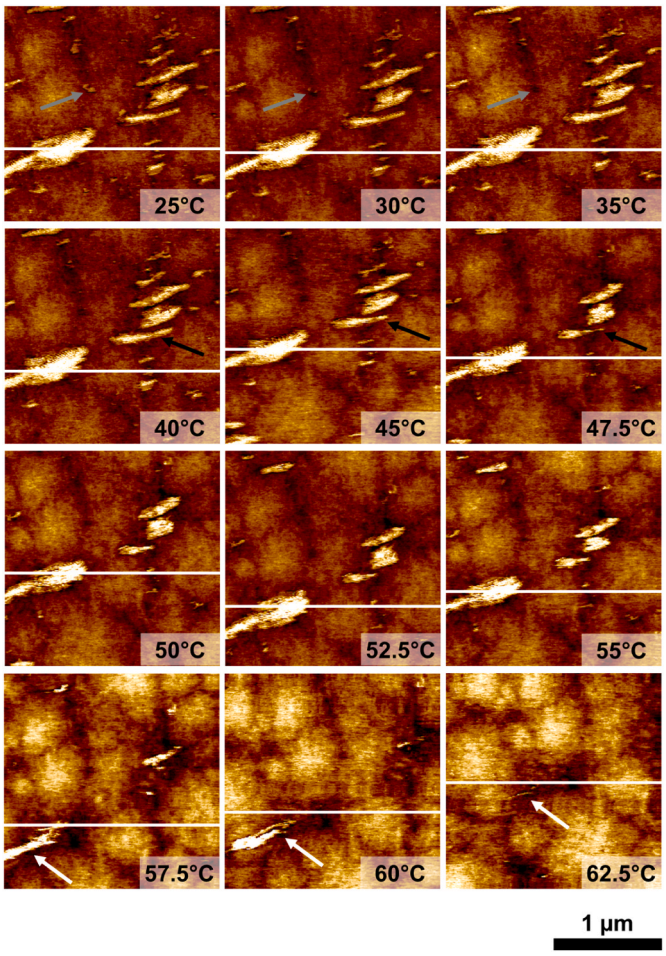

Fig. 4. Consecutive Young's modulus maps captured at the same spot for the PU_{PCL} sample at elevated temperatures, as indicated. Note that the color scales in the maps are adjusted individually to unveil all surface features (absolute values shall be compared using the cross-section plots). The cross-sections are taken along the white lines and shown in a plot in Fig. 5. Scan size is 2 μm × 2 μm. The arrows point to a selected hard phase feature (discussed in the text). (For interpretation of the references to color in this figure legend, the reader is referred to the Web version of this article.)

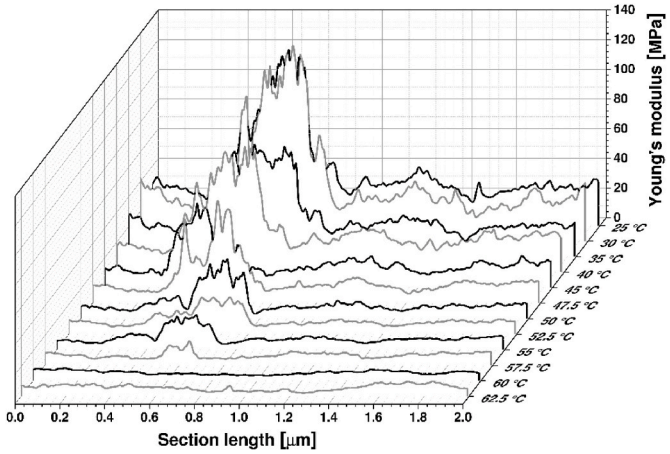

Fig. 5. Cross-section analysis plot for the profiles indicated by white lines in AFM height images shown in Fig. 4.

average Young's modulus value is 6.6 ± 2.1 MPa (Figs. S5 and S6 in the Supporting Information). Interestingly, the sample does not reveal surface growth of the hard domains after cooling down to RT from 65 °C (see Fig. S4 in the Supporting Information).

Set 5: Morphology after heating up to 65 °C (sample re-microtomed). Fig. 6 shows topography images for the PU_{PCL} sample captured at room temperature (21 °C). Prior to this AFM visualization the sample was microtomed, heated up to 65 °C, and re-microtomed. The observed morphology develops at RT over the timescale of days. It should be noted that the second microtoming was performed only to remove the top part of the material (tens of micrometers).

Three hours after completing the re-microtoming, the sample surface reveals short "whiskers", some already are aligned parallel (hard pre-domain). They start to grow mostly at grooves and in holes made by the microtome knife (black arrows in Fig. 6a) but reach sizes smaller than ~ 100 nm (inset in Fig. 6a). One day after re-microtoming, hard domains of varied sizes (elongated up to ~ 1 μm in length) are visible and undergo a growth perpendicular to the microtoming direction. After the second day, the hard domains are elongated above ~1 μm in length. At the fifth day after re-microtoming, some hard domains exceed ~2 μm in length. As in the case of the disappearance of the hard domains at elevated temperatures, their growth is also anisotropic; slow along the microtome cutting direction, but fast perpendicular to this direction. The growth is also present in a vertical direction (height), which can be observed in the topography scale bar (Fig. 6).

The surface-initiated growth results in a variation of the AFM surface coverage of the hard domains versus time, as shown in Fig. 7. The surface coverage increases relatively fast between day 0 and day 2 (1.9, 12.1, 22.9%), and at a slower rate between day 2 and day 14 (22.9, 38.9, 70.7%).

Fig. 8 shows hard domains merging over time at room temperature, as unveiled by surface modulus imaging. "Whiskers" aligned in parallel are visible. White arrows indicate steps in the merging process.

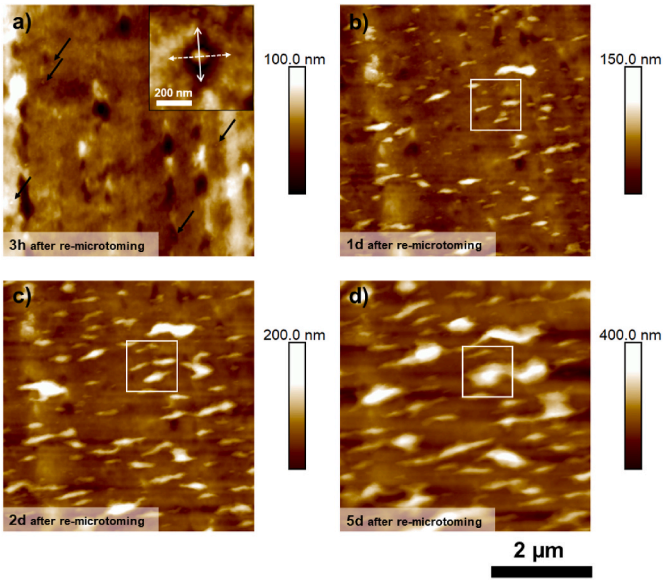

Fig. 6. AFM height images captured at room temperature (21 °C) for the PU_{PCL} sample, previously, microtomed, heated up to 65 °C, and again microtomed (re-microtomed). Images (a), (b), (c) and (d) were collected 3h (0 day), 1 day, 2 days, and 5 days after re-microtoming, respectively. In the area within the white frame, morphological changes at the same spot can be observed. Black arrows in (a) represent chosen nucleation sites (an example is shown in the inset). In the inset the white arrows indicate the direction of microtoming (line) and the direction of the fastest surface growth of the hard domains (dashed). White squares shown in (b), (c) and (d) address areas shown in more details in Fig. 8.

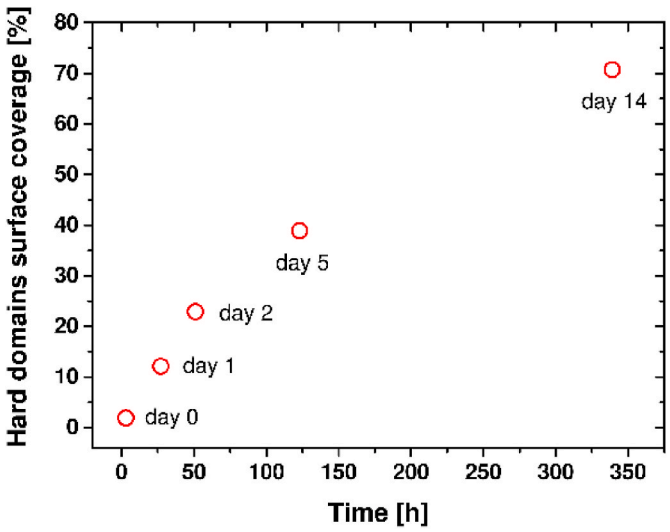

Fig. 7. Surface-initiated growth of hard domains: AFM surface coverage as function of time.

4. Discussion

Let us now consider the free surface of the PU_{PCL} sample (Fig. 2) that has not experienced shear. The hard domains are small and grown in a randomized direction. We would like to consider nucleation and chain diffusion, as a potential explanation for the observations. MDI-BD nucleation can be induced by material impurities or/and surface fingerprints caused by the mold (the material was compression molded; molds have a microscopically rough surface). Regarding the growth, the surface cannot fully minimize its total surface energy. Chain diffusion is limited by segment mobility, and ultimately by the entanglement of the macromolecules. Small molecules can move freely. But once small segments of a large molecule are "fixed" in a hard domain in the vicinity of the rough sample surface (not microtomed), that limits the mobility of the rest of the chain.

Now we turn our attention to images of the microtomed sections (Fig. 3 and subsequent figures). Following microtoming, hard segments become exposed at the freshly cut, flat surface. This results in a surface reconstruction (ordering) of the hard segments, which pack and decrease the total surface energy. The surface reconstruction (hard domain growth) is visible in the AFM images right after microtoming (as fast as a sample can be prepared and measured). Contrary to the images that were obtained on free sample surfaces (non-microtomed), and in addition to our previous observations [21,30], for the microtomed samples, we see a clear surface anisotropy of the "whiskers" that is similar to the graphoepitaxial orientation: the direction of the "whiskers" consisting of the MDI-DB segments is predominantly perpendicular to the knife cutting direction (Figs. 3 and 4). This growth is visible especially on large scan areas (Fig. 3a and Fig. S1 in the Supporting Information).

WAXD data confirm the conclusions drawn from DSC (Fig. S9 in the Supporting Information). The PU_{PCL} sample shows no crystallization (Fig. 1a). The broad WAXD scattering maximum is related to first neighbor chain-chain packing distances and amorphous scattering [38]. The SAXS spacing value (around 12 nm, Fig. 1b) is associated with the size of the hard segments (MDI-BD) in the bulk. Therefore, we note that as WAXD and SAXS patterns showed no bulk anisotropy, the AFM observed oriented surface texture must be related to surface-near orientation of the hard domains. The bulk is in form of a thermoplastic elastomer. Thus, no large-scale diffusion can occur, and no large hard domains are formed.

We continue our discussion of surfaces observed at elevated temperatures. By choice, the surface area inspected contains a variety of nano-sized to micron-sized hard domains (Fig. 4). As indicated by grey arrows in Fig. 4, small hard domains are dispersed in the soft phase up to 35 °C. We attribute this to the thermodynamic stabilization of the phases. The weakened internal interactions between hard segments and their easier mobility at elevated temperatures facilitate the reorganization of the hard domains [39]. Small domains have more excess free energy, thus are less stable. As a result, smaller structures break apart at lower temperatures (dispersion in PCL-based phase). This conclusion is supported by the DSC and SAXS data. In DSC, the disruption of the hydrogen bonding between hard segments occurs around 160 °C (Fig. S9 in the Supporting Information). Below that temperature, the hard MDI-BD segments should still be stacked by hydrogen bonding interaction but dispersed in the soft phase. In SAXS, the presence of the structural size (~12 nm) in the PU_{PCL} is visible, at least up to the temperature the SAXS was performed at (95 °C). This means the ordered hard segments (MDI-BD segments) are present in the copolymer phase with a few MDI residues, but not in the form of micron- and submicron sized domains, as already stated above [40].

Above 40 °C, the remaining hard domains undergo more effective dispersion in the soft phase (see black arrows in Fig. 4). An interesting observation is the presence of the "ball-like" structures. Similar "ball-like" features were already observed at room temperature for solution casted PUs with MDI-BD segments, preheated at 65 °C (4h) and later heated at 40 °C (6h) in Ref. [15]. The "ball-like" features were hypothesized to be "spherulitic-like". In addition to this work, in our case the "ball-like" structures further occur with temperature. An Example of

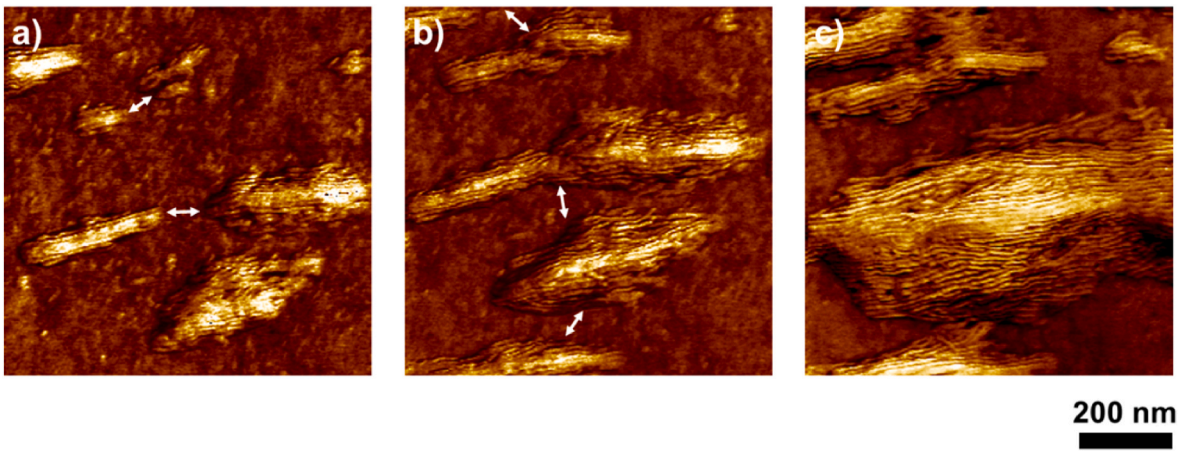

Fig. 8. Young's modulus maps captured at room temperature (21 °C) of the PU_{PCL} sample previously microtomed, heated up to 65 °C, and re-microtomed. Maps (a), (b), and (c) were collected 1 day, 2 days, and 5 days after re-microtoming, respectively.

the sample morphology above 65 °C is shown Fig. S5 in the Supporting Information. Along with morphological variations, the average value of the Young's modulus shows an abrupt change in the temperature range of 40–50 °C (Fig. S7 in the Supporting Information).

Within the temperature range 62.5–65 °C, all hard domains are finely broken up and hard segments are well dispersed at the surface in the soft phase. The miscibility process is extended over 30 °C (35 ÷ 65 °C), probably also due to a significant content of the hard segments and the thermodynamic stability mentioned earlier [21,30]. When reducing the temperature from 65 °C down to RT, the surface morphology surprisingly remains unchanged. The FTIR spectra of the PU_{PCL} sample before heating to 65 °C and after, measured at the room temperature, are identical (Fig. S8 in the Supporting Information). Thus, hydrolysis in the sample does not occur. The AFM height image shows microtome grooves, and the AFM elasticity map still displays the "ball-like" structures (Fig. S4 in the Supporting Information). The hard domains do not grow reversibly with lowering the temperature, or at least this process is very slow (the presence of "ball-like" structures may distort the growth-reversibility).

The last part of our experiment is to show the growth-reversibility of the hard domains initiated by new (second) microtoming. Fig. 6a can be understood as the microtome grooves and scars serve as nucleation sites for the hard segments to build new domains. Due to high chain-mobility of the PCL phase (amorphous), the MDI-BD segments can interact with each other and continue the surface-initiated growth of hard domains (Fig. 6a–c). The "whiskers" and thus the hard domains occur anisotropically: slow along the microtome cutting direction, but fast perpendicular to this direction; vertical growth occurs as well. All together these phenomena are similar to a graphoepitaxial nucleation mechanism [26,41,42]. The "whiskers" are mostly oriented parallel to each other; their direction of growth varies only slightly as shown in Fig. 8. This variation in the direction of growth is probably due to orientation of the nucleation centre (nuclei) in the initial phase of the domain growth or/and defects in the stacking abilities of the MDI-BD molecular segments.

5. Summary and conclusion

We have studied the nanoscale order-disorder transitions of MDI-BD hard segments in a polycaprolactone-based polyurethanes. The studies were conducted primarily by AFM with the focus on free (molded, with no shear history), and bulk surfaces (microtomed, with shear history) at elevated temperatures. At room temperature (RT), the MDI-BD hard segments are stacked to form "whiskers" (10–15 nm in width, but of different length), which are ordered and aligned to compose hard domains. At the free surface and at RT, the growth of the "whiskers" is randomized, and the chain diffusion is limited so that only small hard domains occur. At the bulk surface and at RT, the hard domains grow perpendicularly to the microtome knife movement direction. This anisotropic behavior is like the graphoepitaxial nucleation mechanism. At elevated temperatures, small hard domains have more excess free energy, thus they break apart before larger hard domains do. At 65 °C all hard domains are finely broken down and MDI-BD hard segments are well dispersed in the soft phase, however aggregating into "ball-like" structures. After cooling the sample down to RT, the "ball-like" structures are still present on the surface, and surprisingly no evidence of nucleation of "whiskers" is found. However, the "whiskers" and the domains grow reversibly upon re-microtoming.

(Cryo)microtoming is one of the most important methods of preparing samples of polymeric materials for microscopic measurements, including AFM. Our experiments show, however, that the growth can be initiated at the surface by microtome-engraving. Therefore, when preparing samples, especially those polymers that show phase separation ability, it is important to pay attention to the elapsed time between completing the microtome cutting and microscopic measurement. Moreover, slight increases in ambient temperature can also result in rearrangements of the polymer chains and occur already far from the glass transition/melting temperatures.

Declaration of competing interest

The authors declare that they have no known competing financial interests or personal relationships that could have appeared to influence the work reported in this paper.

Data availability

Data will be made available on request.

Acknowledgment

The authors acknowledge the University of Twente for funding.

Appendix A. Supplementary data

Supplementary data to this article can be found online at https://doi.org/10.1016/j.polymertesting.2023.107961.

References

[1] P. Król, Synthesis methods, chemical structures and phase structures of linear polyurethanes. Properties and applications of linear polyurethanes in polyurethane elastomers, copolymers and ionomers, Prog. Mater. Sci. 52 (2007) 915–1015.
[2] C.J. Paul, M.R. Gopinathan Nair, N.R. Neelakantan, P. Koshy, B.B. Idage, A. A. Bhelhekar, Segmented block copolymers of natural rubber and 1, 3-butanediol-toluene diisocyanate oligomers, Polymer 39 (1998) 6861–6874.
[3] C. Prisacariu, Structural studies on polyurethane elastomers, in: C. Prisacariu (Ed.), Polyurethane Elastomers: from Morphology to Mechanical Aspects, Springer Vienna, Vienna, 2011, pp. 23–60.
[4] K. Bagdi, K. Molnár, M. Kállay, P. Schön, J.G. Vancsó, B. Pukánszky, Quantitative estimation of the strength of specific interactions in polyurethane elastomers, and their effect on structure and properties, Eur. Polym. J. 48 (2012) 1854–1865.
[5] P. Schön, K. Bagdi, K. Molnar, P. Markus, B. Pukanszky, G.J. Vancso, Quantitative mapping of elastic moduli at the nanoscale in phase separated polyurethanes by AFM, Eur. Polym. J. 47 (2011) 692–698.
[6] B. Pukánszky Jr, K. Bagdi, Z. Tóvölgyi, J. Varga, L. Botz, S. Hudak, T. Dóczi, B. Pukánszky, Nanophase separation in segmented polyurethane elastomers: effect of specific interactions on structure and properties, Eur. Polym. J. 44 (2008) 2431–2438.
[7] H.D. Kim, J.H. Huh, E.Y. Kim, C.C. Park, Comparison of properties of thermoplastic polyurethane elastomers with two different soft segments, J. Appl. Polym. Sci. 69 (1998) 1349–1355.
[8] H. Janik, M. Sienkiewicz, J. Kucinska-Lipka, 9 - polyurethanes A2 - dodiuk, hanna, in: S.H. Goodman (Ed.), Handbook of Thermoset Plastics, third ed., William Andrew Publishing, Boston, 2014, pp. 253–295.
[9] J. Guan, K.L. Fujimoto, M.S. Sacks, W.R. Wagner, Preparation and characterization of highly porous, biodegradable polyurethane scaffolds for soft tissue applications, Biomaterials 26 (2005) 3961–3971.
[10] P.A. Gunatillake, R. Adhikari, N. Gadegaard, Biodegradable synthetic polymers for tissue engineering, Eur. Cell. Mater. 5 (2003) 1–16.
[11] L.H. Chan-Chan, R. Solis-Correa, R.F. Vargas-Coronado, J.M. Cervantes-Uc, J. V. Cauich-Rodríguez, P. Quintana, P. Bartolo-Pérez, Degradation studies on segmented polyurethanes prepared with HMDI, PCL and different chain extenders, Acta Biomater. 6 (2010) 2035–2044.
[12] M. Martina, D.W. Hutmacher, Biodegradable polymers applied in tissue engineering research: a review, Polym. Int. 56 (2007) 145–157.
[13] H. Schönherr, G.J. Vancso, Scanning Force Microscopy of Polymers, Springer, Heidelberg, 2010.
[14] D. Wang, T.P. Russell, Advances in atomic force microscopy for probing polymer structure and properties, Macromolecules 51 (2018) 3–24.
[15] Y. Xu, Z. Petrovic, S. Das, G.L. Wilkes, Morphology and properties of thermoplastic polyurethanes with dangling chains in ricinoleate-based soft segments, Polymer 49 (2008) 4248–4258.
[16] J.P. Sheth, G.L. Wilkes, A.R. Fornof, T.E. Long, I. Yilgor, Probing the hard segment phase connectivity and percolation in model segmented poly(urethane urea) copolymers, Macromolecules 38 (2005) 5681–5685.
[17] A. Aneja, G.L. Wilkes, A systematic series of 'model' PTMO based segmented polyurethanes reinvestigated using atomic force microscopy, Polymer 44 (2003) 7221–7228.
[18] R.S. McLean, B.B. Sauer, Tapping-mode AFM studies using phase detection for resolution of nanophases in segmented polyurethanes and other block copolymers, Macromolecules 30 (1997) 8314–8317.
[19] J.T. Garrett, C.A. Siedlecki, J. Runt, Microdomain morphology of poly(urethane urea) multiblock copolymers, Macromolecules 34 (2001) 7066–7070.

[20] E. Tocha, H. Janik, M. Dębowski, G.J. Vancso, Morphology of polyurethanes revisited by complementary AFM and TEM, J. Macromol. Sci. Phys. 41 B (2002) 1291–1304.
[21] H. Gojzewski, B. Imre, C. Check, R. Chartoff, G.J. Vancso, Mechanical mapping and morphology across the length scales unveil structure–property relationships in polycaprolactone based polyurethanes, J. Polym. Sci. B 54 (2016) 2298–2310.
[22] B. Imre, D. Bedo, A. Domján, P. Schön, G.J. Vancso, B. Pukánszky, Structure, properties and interfacial interactions in poly(lactic acid)/polyurethane blends prepared by reactive processing, Eur. Polym. J. 49 (2013) 3104–3113.
[23] R. Pearce, G.J. Vancso, Real-time imaging of melting and crystallization in poly (ethylene oxide) by atomic force microscopy, Polymer 39 (1998) 1237–1242.
[24] G. Reiter, J.U. Sommer, Crystallization of adsorbed polymer monolayers, Phys. Rev. Lett. 80 (1998) 3771–3774.
[25] D. Pires, J.L. Hedrick, A. De Silva, J. Frommer, B. Gotsmann, H. Wolf, M. Despont, U. Duerig, A.W. Knoll, Nanoscale three-dimensional patterning of molecular resists by scanning probes, Science 328 (2010) 732–735.
[26] L.G.M. Beekmans, G.J. Vancso, Real-time crystallization study of poly (ε-caprolactone) by hot-stage atomic force microscopy, Polymer 41 (2000) 8975–8981.
[27] A. Agnihotri, J.T. Garrett, J. Runt, C.A. Siedlecki, Atomic force microscopy visualization of poly(urethane urea) microphase rearrangements under aqueous environment, J. Biomater. Sci. Polym. Ed. 17 (2006) 227–238.
[28] B.K. Kim, S.Y. Lee, M. Xu, Polyurethanes having shape memory effects, Polymer 37 (1996) 5781–5793.
[29] H. Ur Rehman, Y. Chen, M.S. Hedenqvist, H. Li, W. Xue, Y. Guo, Y. Guo, H. Duan, H. Liu, Self-healing shape memory PUPCL copolymer with high cycle life, Adv. Funct. Mater. 28 (2018).
[30] B. Imre, H. Gojzewski, C. Check, R. Chartoff, G.J. Vancso, Properties and phase structure of polycaprolactone-based segmented polyurethanes with varying hard and soft segments: effects of processing conditions, Macromol. Chem. Phys. 219 (2018), 1700214.
[31] M.E. Dokukin, I. Sokolov, Quantitative mapping of the elastic modulus of soft materials with HarmoniX and PeakForce QNM AFM modes, Langmuir 28 (2012) 16060–16071.
[32] W. Walczyk, P.M. Schön, H. Schönherr, The effect of PeakForce tapping mode AFM imaging on the apparent shape of surface nanobubbles, J. Phys. Condens. Matter 25 (2013).
[33] J.L. Hutter, J. Bechhoefer, Calibration of atomic-force microscope tips, Rev. Sci. Instrum. 64 (1993) 1868–1873.
[34] J.E. Sader, I. Larson, P. Mulvaney, L.R. White, Method for the calibration of atomic force microscope cantilevers, Rev. Sci. Instrum. 66 (1995) 3789–3798.
[35] B.V. Derjaguin, V.M. Muller, Y.P. Toporov, Effect of contact deformations on the adhesion of particles, J. Colloid Interface Sci. 53 (1975) 314–326.
[36] H. Gojzewski, J. Obszarska, A. Harlay, M.A. Hempenius, G.J. Vancso, Designer poly (urea-siloxane) microspheres with controlled modulus and size: synthesis, morphology, and nanoscale stiffness by AFM, Polymer 150 (2018) 289–300.
[37] Bruker, PeakForce QNM User Guide (Ver. 004-1036-000), 2011.
[38] G. Vancso, D. Snétivy, I. Tomka, Structural changes during polystyrene orientation: a study of optical birefringence and wide angle X-ray scattering, J. Appl. Polym. Sci. 42 (1991) 1351–1359.
[39] X. Li, Y. Lu, H. Wang, E. Pöselt, B. Eling, Y. Men, Crystallization of hard segments in MDI/BD-based polyurethanes deformed at elevated temperature and their dependence on the MDI/BD content, Eur. Polym. J. 97 (2017) 423–436.
[40] J.T. Koberstein, A.F. Galambos, L.M. Leung, Compression-molded polyurethane block copolymers. 1. Microdomain morphology and thermomechanical properties, Macromolecules 25 (1992) 6195–6204.
[41] L.G.M. Beekmans, R. Vallée, G.J. Vansco, Nucleation and growth of poly (ε-caprolactone) on poly(tetrafluoroethylene) by in-Situ AFM, Macromolecules 35 (2002) 9383–9390.
[42] L.G.M. Beekmans, D.W. Van der Meer, G.J. Vancso, Crystal melting and its kinetics on poly(ethylene oxide) by in situ atomic force microscopy, Polymer 43 (2002) 1887–1895.